




Shake table testing of a half-scale stone masonry building aggregate

I. Tomić¹ · A. Penna² · M. DeJong³ · C. Butenweg⁴ · A. A. Correia⁵ · P. X. Candeias⁵ · I. Senaldi⁶ · G. Guerrini² · D. Malomo⁷ · K. Beyer¹ 

Received: 7 June 2022 / Accepted: 29 October 2023
© The Author(s) 2023

Abstract

Masonry aggregates have developed throughout city centres of Europe due to a centuries-long densification process that generally lacked consistent planning or engineering. Adjacent units are connected either through interlocking stones or a layer of mortar. Without interlocking stones, the connection between the units is weak, and an out-of-phase response of the units can lead to separation and pounding. Modelling guidelines and code instructions are missing for modelling the interaction of such adjacent units because of scarce experimental data. Therefore, in this study an unreinforced stone masonry aggregate was tested on the bidirectional shake table with an incremental seismic protocol as a part of the SERA AIMS—Adjacent Interacting Masonry Structures project. The aggregate was constructed at half-scale with double-leaf undressed stone masonry without interlocking between the units. Floors were built with timber beams and one layer of planks, with different beam span orientation for each unit. After significant damage, one of the units was retrofitted by anchoring the timber beams to the walls to prevent out-of-plane failure and testing was continued. Significant interaction between the units was observed with specific damage mechanisms. Cracking and separation were observed at the interface in both longitudinal and transverse direction, starting at lower intensity runs and progressively increasing. Bidirectional seismic excitation affected the unit separation, with friction forces seemingly playing a role in the transverse direction. Signs of pounding at the interface were observed during higher intensity runs, together with the formation of a soft storey mechanism at the upper storey of the higher unit. The mechanism involved an out-of-plane response of the shared wall, with a horizontal crack at the height of the interaction. These findings contribute to a better understanding of the seismic behaviour of masonry aggregates.

Keywords Historical masonry · Masonry aggregates · Shake table test · Seismic performance · Dry joint · Flexible diaphragms



Fig. 1 **a** Example aggregate in Basel, Switzerland; **b** Half-scale masonry aggregate tested at the EUCENTRE

1 Introduction

Historical city centres throughout Europe were developed and densified over centuries in the form of building aggregates, where it is common for adjacent buildings (often referred to as structural units) to share the structural walls that are orthogonal to the streets. This densification process often took place without consistent planning or engineering, meaning that adjacent buildings can have different material properties, distribution of openings, and floor and roof heights. Facades of adjacent buildings are connected via interlocking and protruding stones or just through vertical mortar joints. Recent earthquakes in Italy showed that the opening of the joint can lead to pounding between the structural units and to complex interacting behaviour (Carocci 2012; da Porto et al. 2013). Therefore, the analysis of masonry building aggregates poses numerous challenges, with no clear or detailed modelling guidelines due to lack of experimental data stemming from the high cost and complexity of performing tests on large-scale aggregates.

Although multiple experimental campaigns were performed on stone masonry buildings (Tomažević et al. 1991; Magenes et al. 1995, 2014; Benedetti et al. 1998; Mazzon et al. 2010; Senaldi et al. 2014; Vintzileou et al. 2015), only a single experimental campaign (Senaldi et al. 2019a; Guerrini et al. 2019) investigated the interaction between the adjacent buildings in an aggregate. A stone masonry aggregate was designed at the University of Pavia, Italy, to reproduce the features typical for the historical centre of Basel, Switzerland, and was tested on the EUCENTRE shake table in Pavia, Italy both in original and strengthened configurations. The aggregate was composed of two adjacent three-storey units that were weakly connected by interlocking stones. The walls were constructed from double-leaf undressed stone masonry. The floors were composed of timber beams and one layer of planks and were therefore assumed to act as flexible diaphragms in their plane. The floor beams of the adjacent units were at the same level; they were connected to each other by steel elements as part of a possible strengthening solution. The specimen was built to half-scale, and the material properties were scaled accordingly to respect the similitude laws, with detailed material characterizations performed before the test (Guerrini et al. 2017; Senaldi et al. 2018). The specimen is shown in Fig. 1.

An incremental, unidirectional dynamic test was performed on the original specimen up to the near-collapse state for a peak ground acceleration (PGA) of 0.35 g, and an out-of-plane mechanism formed in both gables. Portions of longitudinal facades also acted as

flanges due to good interlocking in the corners. Due to the interlocking stones and connected slab beams, little separation between units was detected: the adjacent piers belonging to different units behaved as one, forming a wide central pier. However, these high-quality connections, ensured by good workmanship on a carefully constructed laboratory specimen, can be updated and extended to represent the wide range of masonry quality found in actual city centres. For instance, units can also be connected by only a vertical layer of mortar without interlocking stones, which can further weaken the aggregate interface. Additionally, floor levels can be at different heights and timber beams of adjacent units cannot be connected. Finally, bidirectional excitation can trigger a more complex response of the aggregate interface.

In the past numerical studies on masonry aggregates, the units were modelled as fully coupled (Senaldi et al. 2010; Formisano et al. 2015; Maio et al. 2015; Formisano 2017; Formisano and Massimilla 2018). In some cases, they were also modelled in parallel as fully separated to compare the responses (Senaldi et al. 2010; Formisano et al. 2015; Formisano and Massimilla 2018). In other cases, a part of an aggregate was modelled separately with the rest of the aggregate accounted for through modelling of springs (Formisano and Massimilla 2018), rod and foundation elements (Stavroulaki 2019) or restraints (Malcata et al. 2020). For the large-scale seismic vulnerability assessment of masonry building aggregates, Formisano et al. (2015) numerically calibrated a procedure derived from the well-known existing vulnerabilities of masonry buildings (Benedetti and Petrini 1984; Benedetti et al. 1998): this procedure integrated five parameters accounting for the aggregate conditions, which were the presence of adjacent buildings with different heights, the position of the unit in the aggregate, the number of staggered floors, the structural or typological heterogeneity among adjacent structural units, and the different percentages of opening areas among adjacent facades. Numerical calibration and validation were performed with an equivalent-frame method (EFM) using the software 3Muri (S.T.A. Data 2008) by subjecting the two case-study aggregates and single units to several pushover analyses. The units were modelled as fully connected.

Different studies reached different conclusions, i.e., Senaldi et al. (2010) concluded that the impact of aggregate behaviour in the transverse direction can be ignored, while Formisano and Massimilla (2018) came to the same conclusion for the longitudinal direction. However, in all these cases, reference analyses performed on entire masonry aggregates modelled the units of the aggregate as perfectly connected. Modelling fully coupled units leads to wide piers at the interface of the units and overestimates the interface strength and stiffness, especially if built with weak or no interlocking. Conversely, modelling fully separated units can result in either a conservative or nonconservative approximation, depending both on the position of each unit in the aggregate and on the material and geometrical properties of the neighbouring units (Senaldi et al. 2010; Formisano et al. 2015).

To assess the capability of the EFM to capture the experimental response of masonry aggregates, the University of Pavia's test was modelled by Senaldi et al. (2019b) with the software Tremuri (Lagomarsino et al. 2013), using a macro-element developed by Penna et al. (2014). The two units were modelled as fully connected with a continuous wide pier at the interface. Numerical and experimental results were compared in terms of pushover and backbone curves, hysteretic responses, lateral displacement profiles, damage patterns and failure mechanisms. The pushover curve estimated the lateral strength well but overestimated the global stiffness of the aggregate. The dynamic analysis, instead, estimated the hysteretic response well but underestimated the displacement demand. However, the overestimation of the global stiffness was attributed more to the EFM difficulty in reproducing the out-of-plane response, rather than to a perfect connection between the units in

the model. In fact, the specimen had interlocking stones across the interface, and the floor beams of adjacent units were at the same level and connected.

This same aggregate was modelled by Vanin et al. (2020a) using a newly developed macro-element (Vanin et al. 2020b) implemented in the OpenSEES software (McKenna et al. 2000). The approach accounted for both in-plane and out-of-plane behaviour and the nonlinearity of floor-to-wall and wall-to-wall connections. The two units were modelled as perfectly connected. After calibrating it based on an experimental campaign, the model satisfactorily predicted the failure mode, displacement, and distribution of drift values in the piers. However, it was highly sensitive to parameters such as damping ratio and floor-to-wall friction coefficient, especially for higher levels of seismic excitation.

The lack of advanced modelling approaches for the interface between the units might be due to the absence of experimental data on their typologies and behaviour. The need for experimental data prompted a joint research programme named SERA AIMS—Adjacent Interacting Masonry Structures, between the École Polytechnique Fédérale de Lausanne (EPFL), Switzerland; the University of Pavia, Italy; the University of California, Berkeley, USA; the RWTH Aachen University, Germany; and the National Laboratory for Civil Engineering (LNEC), Portugal. To fill the knowledge gaps and contribute to the understanding of the behaviour of masonry building aggregates, a test unit was designed with the assistance of numerical modelling, to meet these goals:

- Induce opening of the interface between the units;
- Aim for a global behaviour sensitive to the interface behaviour (i.e., numerical results are sensitive to the modelling assumptions with regard to the interface between units);
- Modal properties differ between fully connected units (elastic interface for the modal analysis) and isolated units (separate units);
- Avoid premature out-of-plane collapse;
- Fit within the geometrical and payload limitations of the shake table.

The following sections describe the specimen geometry, material properties, construction details, masses, and strengthening interventions. The input ground motion is presented along with the loading sequence. Results are presented in terms of crack maps and damage mechanisms, interface behaviour, in-plane facade elongations, and force–displacement responses. Finally, the data are discussed with the aim of enhancing the understanding of historical masonry aggregates behaviour.

2 Specimen description

The specimen was constructed as a half-scale stone masonry aggregate consisting of two units. The orientation of the units with respect to the x – y reference system and the labels of the walls are shown in Fig. 2. Masonry typology and material properties reproduced, as much as possible, those of the aggregate tested by the University of Pavia (Senaldi et al. 2019a; Guerrini et al. 2019). The construction sequence replicated that of historical city centres such that Unit 2 was constructed before Unit 1 to ensure no interlocking between the units at any given height.

The main dimensions are shown in Fig. 3. Unit 1 had a single storey with a height of 2.2 m, while Unit 2 had two storeys with heights of 1.65 m and 1.5 m, respectively, for a total height of 3.15 m. Unit 1 had a U-shaped three-wall layout with plan dimensions of

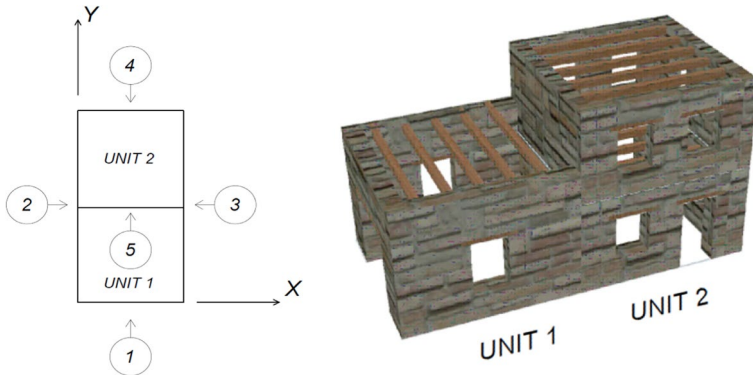


Fig. 2 Unit orientation and facade numbering of the half-scale stone masonry aggregate tested in this study

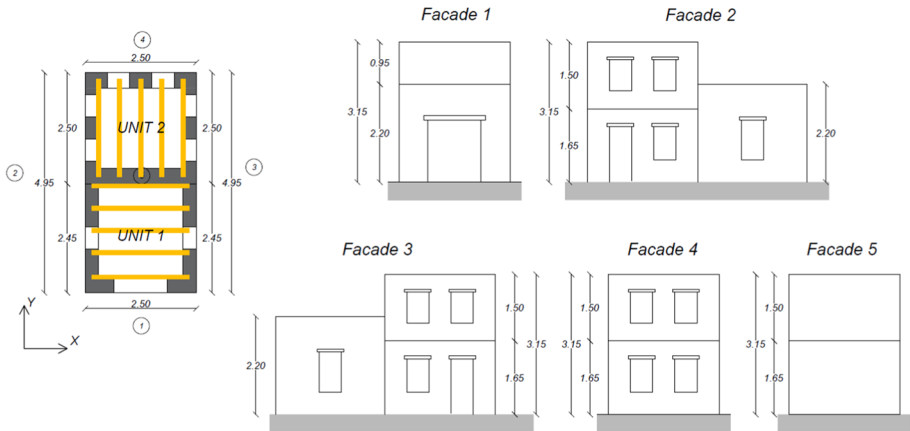


Fig. 3 Plan view and elevations with dimensions of the half-scale stone masonry aggregate tested in this study. Units of m

$2.5 \times 2.45 \text{ m}^2$. Unit 2 was rectangular with four walls and plan dimensions of $2.5 \times 2.5 \text{ m}^2$. Unit 1 had a wall thickness of 30 cm, while Unit 2 had wall thicknesses of 35 cm and 25 cm for the first and second storeys, respectively. The thickness of the spandrels was decreased to 15 cm underneath the openings.

To finish the building, a layer of plaster was applied using mortar of class NHL 2.0, without fibres. The plaster thickness depended on the surface roughness and was approximately 15 mm on average. A layer of paint was applied afterwards to make cracks more visible. The specimen is shown in Fig. 4 before and after application of plaster, paint, and additional masses of Unit 2.

2.1 Masonry properties

The maximum payload of the shake table limited construction of the specimen to half-scale. The specimen scale was commonly reduced in previous experimental campaigns

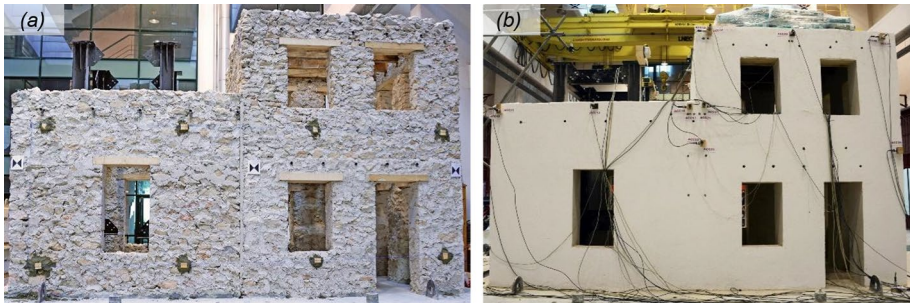


Fig. 4 Facade 3 of the half-scale stone masonry aggregate specimen: **a** Without plaster, paint, and additional masses; **b** Completed test specimen

to research the seismic response of unreinforced masonry buildings (Tomažević et al. 1991; Benedetti et al. 1998; Croci et al. 2010; Mazzon et al. 2010; Vintzileou et al. 2015; Mouzakis et al. 2018). However, when conducting a dynamic test on a scaled model, it is necessary to meet similitude relationships to obtain physically sound results (Buckingham 1914; Krawinkler and Moncarz 1981; Sullivan et al. 2004; Coutinho et al. 2016). Common similitude relationships, such as Cauchy's or Cauchy-Froude's, were not applicable, as the former requires scaling the gravity acceleration, which was unfeasible, and the latter requires increasing the material density, which increases the specimen weight and was also unviable. Consequently, the scale factors used by Guerrini et al. (2019) and Senaldi et al. (2019a) were adopted.

Walls were constructed as double-leaf stone masonry without interlocking between the leaves, except for through stones placed at opening edges and building corners, as shown in Fig. 5. Stone scraps mixed with mortar filled the voids between the leaves, which amounted to about 10% of the volume. The construction material reproduced the University of Pavia's shake table test as much as possible (Senaldi et al. 2019a; Guerrini et al. 2019), to facilitate numerical model calibrations. Table 1 summarises the material properties of the mortar and masonry, with those of the University of Pavia's specimen (Guerrini et al. 2017; Senaldi et al. 2018). Three-point bending, and compression tests were performed on mortar specimens after curing for 28 days. To derive masonry compressive and tensile strength, three vertical and three diagonal compression tests were performed on masonry wallettes, 17 months after their construction and nine months after the shake table test. The shake table test was carried out 8 months after completion of the half-scale aggregate. The delay in material and shake-table testing was due to the pandemic.

Due to differences in stone quarries, it was impossible to exactly replicate the stone type and shape that had been used for the test in Pavia. Therefore, the specimen was constructed with more irregular stones than those used in Pavia, which increased the irregularity of the masonry texture. The stones ranged in size from 10 to 25 cm and were arranged in approximately horizontal courses. The mortar was a commercial hydraulic lime mix, with EPS spheres added in 2:3 volumetric ratio. The EPS spheres were used to half the stiffness and strength of the masonry material (Croci et al. 2010; Moss and Crosariol 2013; Zheng et al. 2016) thus meeting the adopted similitude law (Senaldi et al. 2019a; Guerrini et al. 2019).

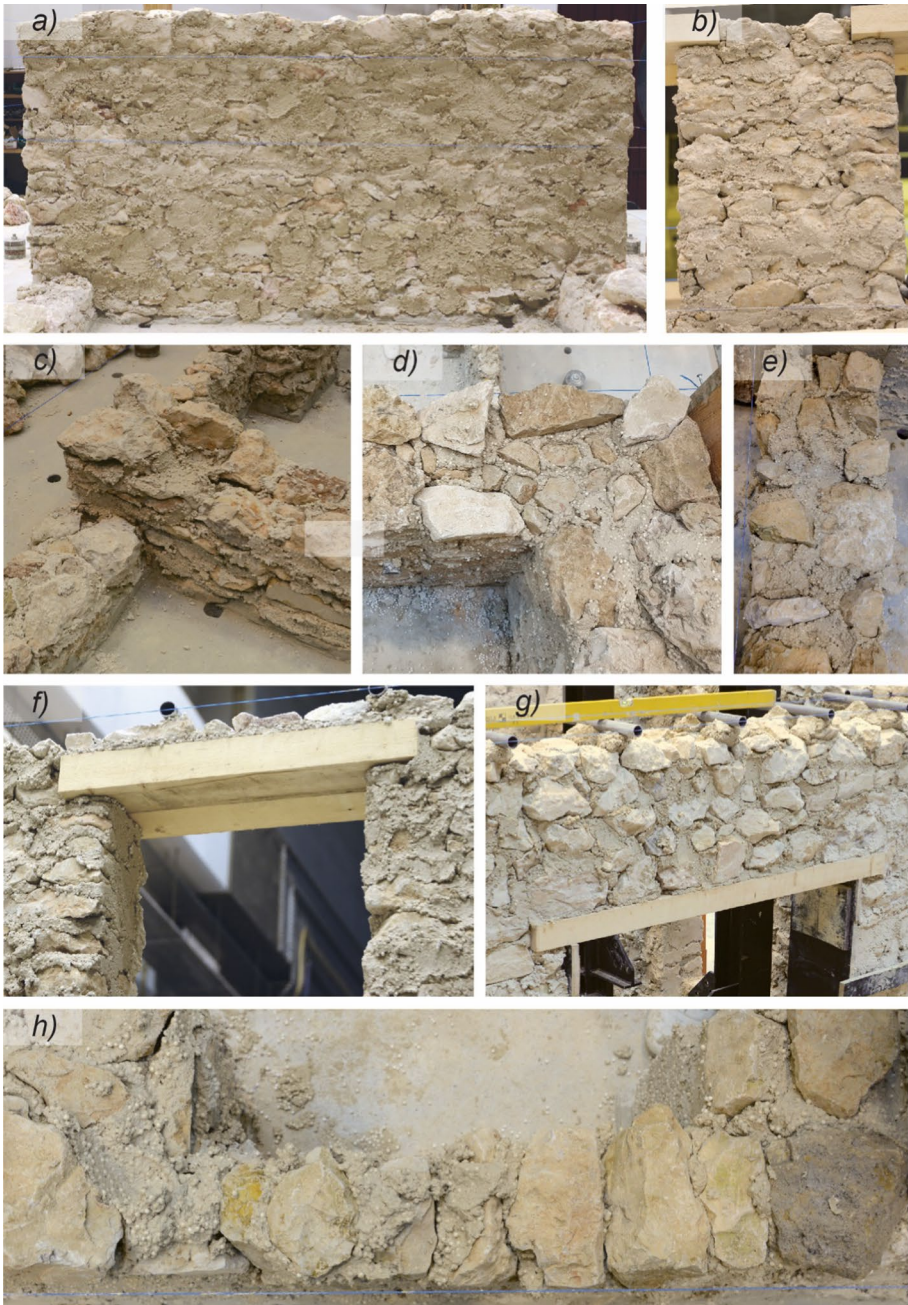


Fig. 5 Masonry typology: **a-b** Masonry texture; **c-d** Construction detail of a corner; **e** Horizontal section; **f** Detail of a lintel; **g-h** Construction detail of a spandrel

Table 1 Mortar and masonry mechanical properties of the University of Pavia's (Guerrini et al. 2017; Senaldi et al. 2018) and the SERA-AIMS test specimens

Value	Univ. of Pavia	SERA-AIMS
Mortar compressive strength f_c		
Average [MPa]	1.75	1.28
Coefficient of variation	0.28	0.284
Mortar flexural strength f_{ct}		
Average [MPa]	0.60	0.66
Coefficient of variation	0.23	0.200
Masonry compressive strength f_m		
Average [MPa]	1.30	1.37
Coefficient of variation	0.026	0.18
Masonry tensile strength f_t		
Average [MPa]	0.17	0.21
Coefficient of variation	0.073	0.05
Masonry cohesion c		
Average [MPa]	0.23	0.29
Coefficient of variation	0.073	0.05

2.2 Interface between units

The two structural units constituting the aggregate were connected by mortar alone without interlocking stones. Unit 2 was constructed first as the older unit of the aggregate. The contact surface of Unit 2 was smoothed with a layer of mortar before constructing the adjacent facades of Unit 1, which ensured no interlock between the units. This detail was chosen to facilitate separation during the test and to create a clearly defined boundary condition between the two units. Figure 6 shows the interface between the units.

2.3 Floor structures

Floors were composed of wooden beams with a cross-section of 8×16 cm that were simply supported on the masonry walls (Fig. 7). The beam support length was 20 cm for the 1st storey of Unit 2, and 15 cm for both Unit 1 and the 2nd storey of Unit 2. Unit 1 beams



Fig. 6 Interface between the units in the stone masonry aggregate specimen



Fig. 7 Beam supports at the 1st floor of Unit 2 of the masonry aggregate specimen

spanned in the transverse direction (x-direction). Unit 2 beams spanned in the longitudinal direction (y-direction; the coordinate system is shown in Fig. 2). A single layer of 2 cm thick planks was placed perpendicularly to the beams and connected by two nails at each intersection. PVC tubes were placed in the walls at the end of each beam and along each edge-beam, to be used in a later phase of the test to install precaution against out-of-plane collapse of the walls.

2.4 Strengthening

PVC tubes were placed in the walls of both units, under each beam support and along beams running parallel next to walls, to allow locally strengthening of the structure. Strengthening included steel angles fastened to the beams and steel bearing plates on the wall outer surfaces, connected though the walls by threaded rods inserted within the PVC tubes. The rods were manually post-tensioned. The details of the intervention are shown in Fig. 8. These improved connections between beams and walls can contrast out-of-plane mechanisms and ensure a box-type behaviour of the building. Strengthening measures were installed after Run 2.1, during which the onset of out-of-plane wall overturning was observed on Unit 2, as shown later in Table 4.

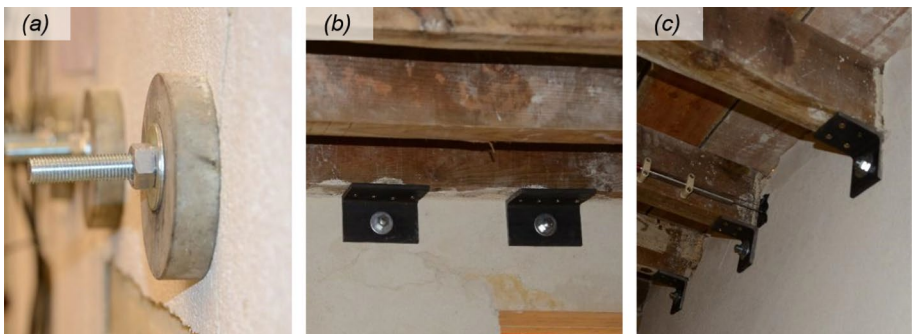


Fig. 8 Details of the strengthening interventions against out-of-plane wall overturning: **a** Bearing plate connection on the exterior of the wall; **b** Steel angles along the edge beam parallel to the wall; **c** Steel angles at the beam supports

2.5 Masses

The total mass of Unit 1 was 7434 kg. The structural mass of Unit 2 was 13,272 kg; additional 1500 kg from steel plates and concrete bags were evenly distributed on each floor of Unit 2, bringing its total mass to 16,272 kg. This increased the differences in modal properties between the units without exceeding the payload limits of the shake table. The stiff steel–concrete foundation added 18,000 kg to the total mass of the aggregate, as shown in Table 2.

3 Seismic input and loading sequence

The aggregate specimen was tested under one- and two-component excitations, using the horizontal records of the 1979 Montenegro earthquake from the Ulcinj-Hotel Albatros station (Luzi et al. 2016). These ground motions are plotted in Fig. 9 as time series and in Fig. 10 as elastic response spectra, with time and periods scaled according to the similitude law (Senaldi et al. 2019a; Guerrini et al. 2019). The east–west component was applied in the longitudinal direction (positive y-direction), and the north–south component in the transverse direction (negative x-direction).

For a structure the size of the AIMS specimen, the shake table capacity was 0.875 g in the longitudinal and 0.62 g in the transverse direction. Four incremental steps were initially planned for the input motions, to reach peak ground accelerations (PGA) of 25%, 50%, 75% and 100% of the shake table capacity in the longitudinal direction, maintaining the original acceleration ratio between the two components. Each step consisted of three stages, i.e., an initial unidirectional test in the longitudinal direction, then a unidirectional test in the transverse direction, and finally a bidirectional test, as shown in Table 3. The actual testing sequence comprised ten overall runs, as shown in Table 4. To improve the calibration of the shake table, three runs at 12.5% of the table capacity were added at the beginning. Widespread damage after Run 7 (2.1) required strengthening Unit 2 before resuming. The sequence was interrupted at step 2, with PGA nominally equal to 50% of the table capacity. Intermediate dynamic identification tests were carried out to track the modal properties of the units.

For Run 2.1 and Run 2.1S in y-direction, the target PGA was 0.438 g, but 35% and 40% greater PGAs were applied (0.593 g and 0.615 g). The overshoot in spectral acceleration spanned across the entire period range up to 0.8 s; as a result, for an estimated

Table 2 Mass breakdown for the masonry aggregate specimen

Component	Mass [kg]
Walls of unit 1	7270
Floors of unit 1	164
Total unit 1	7434
Walls of unit 2	12,937
Floors of unit 2	335
Additional masses of unit 2	3000
Total unit 2	16,272
Steel–concrete foundation	18,000
TOTAL	41,706

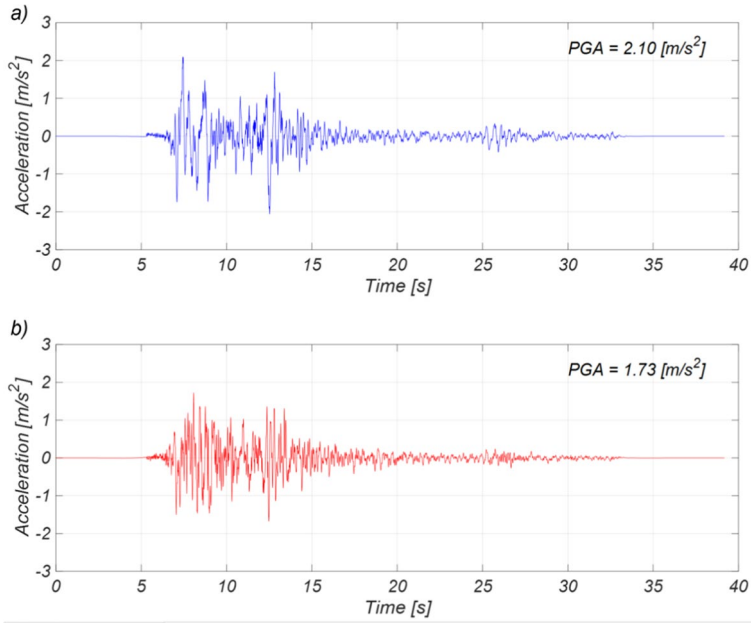


Fig. 9 Processed acceleration time histories of the Montenegro 1979 earthquake recorded at the Ulcinj-Hotel Albatros station, with the scaled time step: **a** East–west component and **b** North–south component

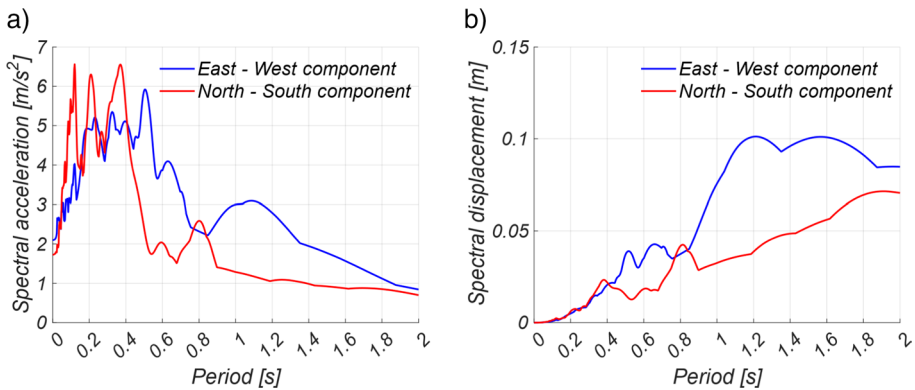


Fig. 10 Elastic response spectra of the Montenegro 1979 earthquake recorded at the Ulcinj-Hotel Albatros station for 5% damping ratio, with the scaled period: **a** Acceleration and **b** Displacement

fundamental period $T=0.13$ s, the actual spectrum of Run 2.1 resembled that of nominal Run 3.1 at 75% of the shake table capacity. Actual Run 2.2S in x-direction was also affected by a 35% overshoot in terms of PGA, but the issue was limited to periods shorter than 0.2 s where the response spectrum approached that of nominal Run 2.3 Response spectra for nominal and actual records are compared on Fig. 11.

Table 3 Planned testing sequence

Run ID	Direction	Level of shaking (w.r.t. longitudinal table capacity)	Nominal PGA (direction) [g]
1.1	Longitudinal	25%	0.219 (y)
1.2	Transverse	25%	0.156 (x)
1.3	Bidirectional	25%	0.219 (y); 0.156 (x)
2.1	Longitudinal	50%	0.438 (y)
2.2	Transverse	50%	0.313 (x)
2.3	Bidirectional	50%	0.438 (y); 0.313 (x)
3.1	Longitudinal	75%	0.656 (y)
3.2	Transverse	75%	0.469 (x)
3.3	Bidirectional	75%	0.656 (y); 0.469 (x)
4.1	Longitudinal	100%	0.875 (y)
4.2	Transverse	100%	0.625 (x)
4.3	Bidirectional	100%	0.875 (y); 0.469 (x)

Table 4 Actual testing sequence

Run ID	Direction	Level of shaking (w.r.t. longitudinal table capacity)	Nominal PGA (direction) [g]	Actual PGA (direction) [g]
Unstrengthened specimen				
0.1	Longitudinal	12.5%	0.110	0.113 (y)
0.2	Transverse	12.5%	0.078	0.075 (x)
0.3	Bidirectional	12.5%	0.110 (y); 0.078 (x)	0.114 (y); 0.072 (x)
1.1	Longitudinal	25%	0.219	0.170 (y)
1.2	Transverse	25%	0.156	0.178 (x)
1.3	Bidirectional	25%	0.219 (y); 0.156 (x)	0.208 (y); 0.174 (x)
2.1	Longitudinal	50%	0.438	0.593 (y)
Strengthened specimen				
2.1S	Longitudinal	50%	0.438	0.615 (y)
1.2S	Transverse	25%	0.156	0.258 (x)
2.2S	Transverse	50%	0.313	0.425 (x)

4 Instrumentation

Forty accelerometers recorded the accelerations of the foundation and the in- and out-of-plane accelerations of the masonry walls. The relative displacement of points were monitored with linear variable displacement transducers (LVDTs) and potentiometers; LVDTs were also used to record the relative displacement between wooden beams and masonry walls. Optotrak LED, Krypton, and Hamamatsu optical measurement systems were used to monitor absolute displacements of chosen points; the absolute displacement measures were used to compute the interface opening between the units. The layout of accelerometers is shown in Fig. 12. The layout of displacement measurements is shown in Fig. 13.

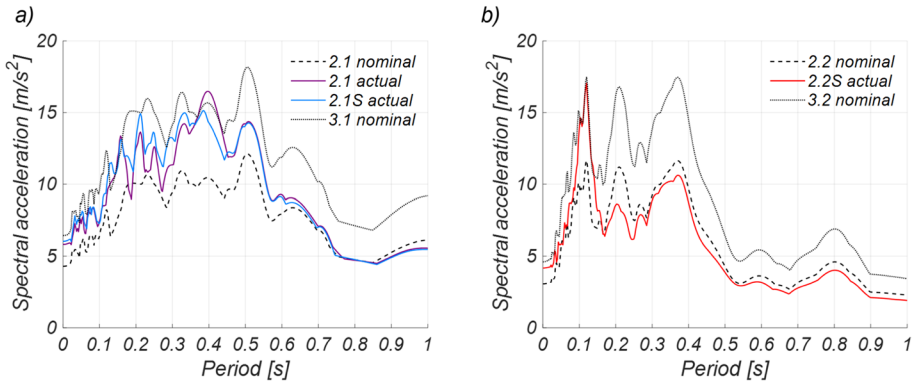


Fig. 11 Comparison of response spectra for selected nominal and actual records: **a** Test runs 2.1 and 2.1S in the longitudinal y -direction; **b** Test run 2.2S in the transverse x-direction

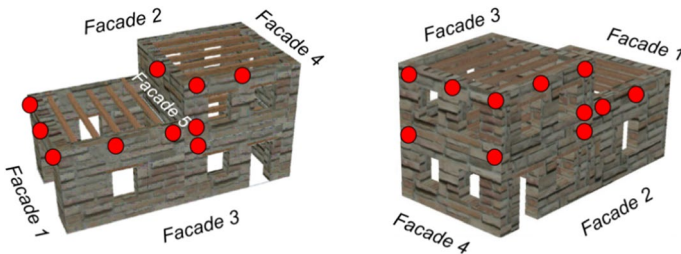


Fig. 12 Layout of accelerometers

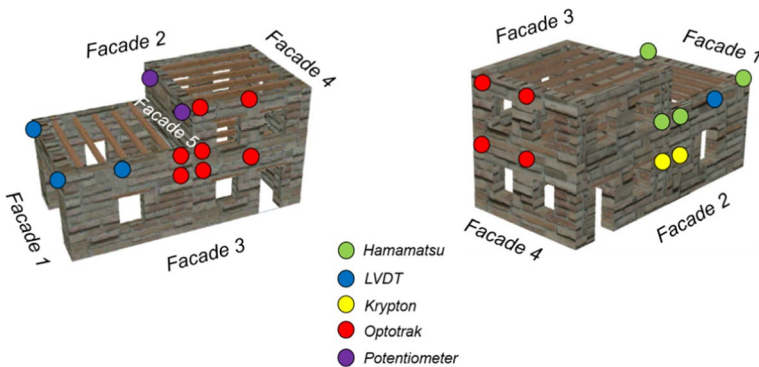


Fig. 13 Layout of LVDTs, potentiometers and optical devices (excluding LVDTs measuring beam-to-wall relative displacement)

5 Results

Test results are first evaluated in terms of crack maps and descriptions of underlying damage mechanisms, interpreting the global behaviour of the aggregate. Then, the interface

behaviour is studied in terms of opening in the longitudinal and transversal direction. Moreover, in-plane elongations of spandrels are studied to interpret the extent of flexural rocking mechanisms of the facades. Finally, force–displacement responses of both units are shown to describe the hysteretic behaviour.

5.1 Damage mechanisms and crack maps

The structural damage sustained by the units was surveyed at the end of every test run. Runs 0.1, 0.2, and 0.3 were performed at 12.5% of the shake table capacity for shake-table calibration purposes, and no damage was detected in any part of the aggregate or at the interface. After the following runs, cracks were mapped on the exterior and interior of each facade to obtain the damage pattern evolution. New cracks observed at the end of each run are marked in colour on the figures, while old cracks in black.

Runs 1.1, 1.2, and 1.3 were performed at 25% of the shake table capacity. The crack maps for these runs are shown in Fig. 14. Blue lines represent damage after run 1.1 (longitudinal run) and red lines represent damage after run 1.3 (bidirectional run). Damage was only detected at the interface between the two units. Optotrak markers placed on both units next to the interface captured the longitudinal and transverse opening of the joint. The maximum opening during run 1.1 was 0.9 mm and 0.2 mm in the longitudinal and transverse directions, respectively. During run 1.3 it was 1.5 mm and 2.7 mm in the same directions, respectively. Signs of minor sliding of the beams above the spandrels at the 2nd storey of Unit 2 were detected after Run 1.3. LVDT data showed that the maximum sliding as well as the residual displacement were 0.1 mm.

Run 2.1, which approached nominal run 3.1 for short period oscillators (Fig. 11), resulted in extensive damage to Unit 2, as shown in the crack maps of Fig. 15 and on the illustrative mechanism of Fig. 16. Cracks on the external and internal sides of the walls were predominantly aligned across the thickness of the walls. An in-plane flexural-rocking mechanism fully formed in both facades 2 and 3 at the upper storey of Unit 2. Spandrels and piers suffered extensive flexural cracking, with maximum residual width of 5.0 mm and 1.4 mm, respectively, at the 2nd storey, and of 1.9 mm and 1.2 mm, respectively, at the 1st storey.

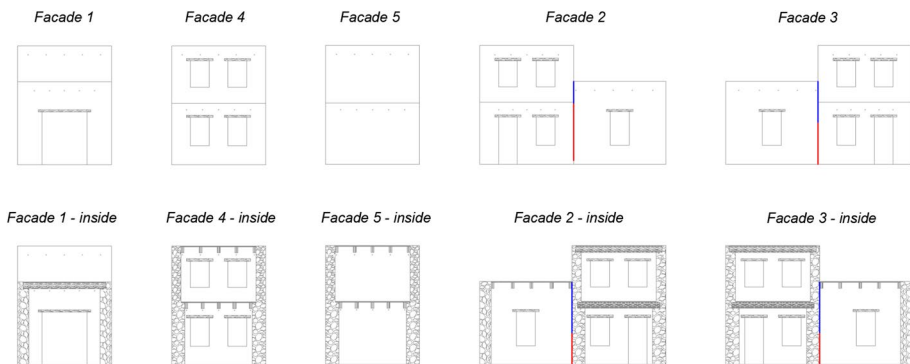


Fig. 14 Crack maps after test runs 1.1, 1.2 and 1.3. Black lines mark previously detected damage; blue lines mark damage observed after run 1.1; red lines mark damage observed after run 1.3

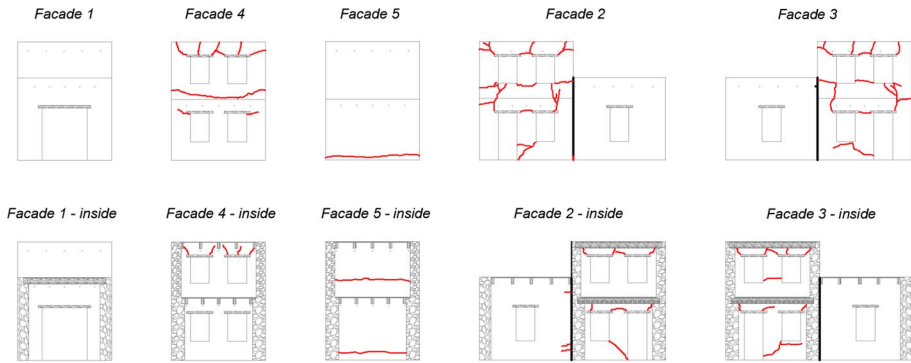
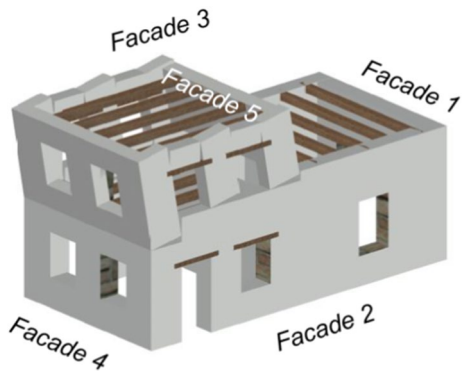


Fig. 15 Crack maps after test run 2.1. Black lines mark previously detected damage; red lines mark damage observed after the current test

Fig. 16 Illustrative deformed shape of Unit 2 for test run 2.1



Out-of-plane cracks were visible at the 1st floor level of facade 4 with residual width up to 0.6 mm, with extensive cracking of the top spandrels of the same facade. Two out-of-plane horizontal cracks were detected on the partition wall (facade 5), at its bottom and at the level of Unit 1 roof. The cracks at the 1st floor level of Unit 2 on facade 4 and the roof level of Unit 1 on facade 5 confirm the interaction with the adjacent unit in the formation of the damage mechanism. Out-of-plane and in-plane cracks were continuous around corners; in fact, thanks to the interlock between orthogonal walls, the end piers of longitudinal facades acted as webs in the out-of-plane overturning mechanism of the transverse walls (Fig. 16).

Signs of sliding of the 2nd floor beams of Unit 2 and residual displacement were also detected. LVDT data showed that the maximum sliding was 4.4 mm and 8.8 mm at the supports of the instrumented beam on facades 4 and 5, respectively, while the residual displacement were 4.3 mm and 8.0 mm, respectively.

Significant interaction, separation and pounding occurred at the interface between the structural units. The maximum recorded openings of the joint were 20.7 mm and 0.6 mm in the longitudinal and transverse directions, respectively. Unit 1 was nearly undamaged, apart from a few hairline cracks that spread horizontally from the interface between units. The damage on facades, interface, and beam supports after run 2.1 are shown in Fig. 17.



Fig. 17 Damage observed at the end of test run 2.1: **a-b** External view of the aggregate; **c** Flexural cracking of a 2nd floor spandrel and at the top of a 2nd storey pier of Unit 2; **d** Cracking and near-detachment of the top of a 2nd storey corner of Unit 2; **e** Flexural cracking of a 1st floor spandrel of Unit 2; **f** Slip of a 2nd floor joist of Unit 2; **g** Damage at the interface between the units; **h** Horizontal crack at the 1st floor level of facade 4 of Unit 2

Unit 2 was retrofitted due to the widespread damage caused by run 2.1, to prevent out-of-plane collapse especially of facade 4. The strengthening was performed by nailing steel angles to the timber beams, installing threaded rods in the PVC tubes, and

fastening them to the steel angles and to steel plates located outside of the walls. Unit 1 instead did not require any strengthening.

To understand the effect of the strengthening intervention, run 2.1 was repeated in this configuration as run 2.1S. The crack maps for this run are shown in Fig. 18. Strengthening prevented out-of-plane failures. After connecting the beams of Unit 2 to the walls, no additional displacement of the beams at their support was expected. However, further sliding was confirmed by the LVDT readings. In fact, the residual displacement of the beams of the 2nd storey of Unit 2 increased to 6.7 mm and 8.6 mm for facades 4 and 5, respectively. This sliding was attributed to the deformation of the masonry, which was already significantly cracked before retrofitting the beam supports.

As cracks in the masonry were not repaired, run 2.1S further amplified the damage mechanism, increasing the width of existing cracks and forming new cracks. Existing cracks at the 2nd storey of Unit 2 increased to a residual width larger than 5.0 mm. A new vertical crack formed inside the partition wall (facade 5) at the centre of the 2nd story, indicating out-of-plane bending. Facade 4 experienced extensive damage at the 1st floor level, with formation of new cracks, widening of old ones, and detachment of portions of plaster. The top corners of the 2nd storey of Unit 2 were severely damaged and almost detached. The 1st storey piers of Unit 2 adjacent to Unit 1 also formed flexural cracks with residual width up to 0.7 mm. Due to interlocking between orthogonal walls, the end piers of the longitudinal facades were still acting as webs in the out-of-plane overturning mechanism of the transverse walls.

Like in the previous run, separation and pounding occurred at the interface between the two units. The maximum recorded openings of the joint were 21.2 mm and 2.0 mm in the longitudinal and transverse directions, respectively.

The following run 1.2S was a repetition of run 1.2 (25% of the shake table capacity), to assess the remaining capacity of the specimen in the transverse direction. However, the run produced no further damage to the specimen.

Finally, the specimen was subjected to run 2.2 in the transverse direction, which approached nominal run 3.2 for short period structures, as shown in Fig. 11. The crack maps for this run are shown in Fig. 19. No new cracks or amplification of previous damage was detected in Unit 2. However, in-plane flexural cracking of the spandrels and piers of facade 1 was observed, as Unit 1 developed the damage mechanism illustrated on Fig. 20.

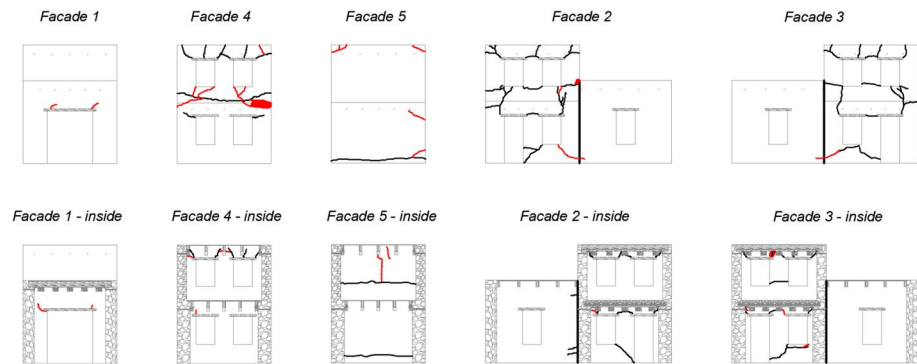


Fig. 18 Crack maps after run 2.1S: black lines mark previously detected damage; red lines mark damage observed after the current test

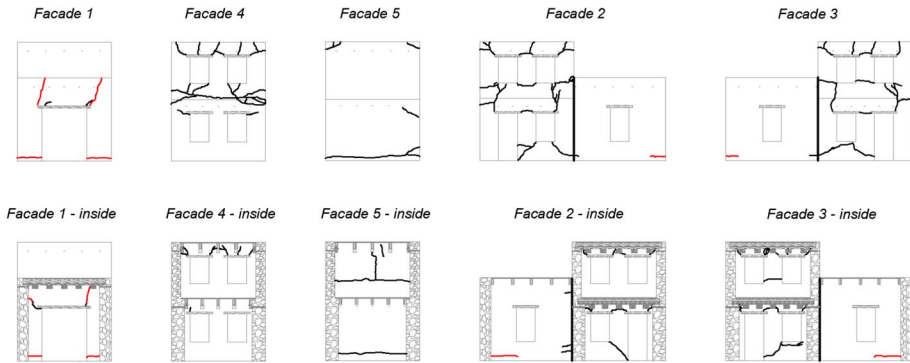


Fig. 19 Crack maps after run 2.2S: black lines mark previously detected damage; red lines mark damage observed after the current test

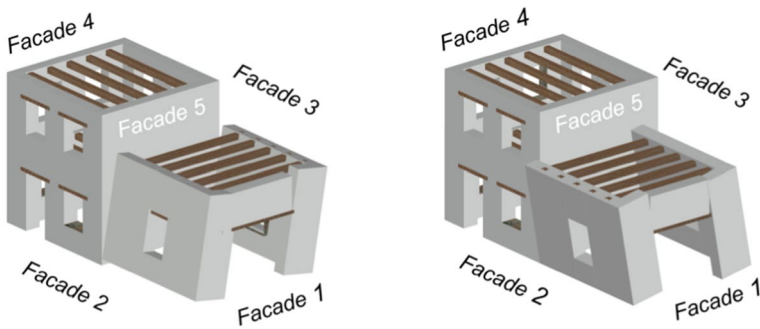


Fig. 20 Illustrative deformed shape of Unit 1 for run 2.2S

The residual crack width was up to 3.0 mm and 1.0 mm for spandrels and piers of facade 1, respectively.

Thin out-of-plane horizontal cracks were observed at the pier bases of facades 2 and 3 in Unit 1. The cracks were continuous around the corners of the building, meaning that the end piers of the transverse facades acted as flanges in the out-of-plane overturning mechanism of the longitudinal walls, thanks to the interlock between orthogonal walls. The maximum residual width of these cracks was 1.0 mm and 0.4 mm for facades 2 and 3, respectively. Indications of beam sliding at the supports were observed and confirmed via LVDT measurements, which showed residual displacements of 1.0 mm and 3.3 mm on facade 2 and facade 3, respectively.

With the failure mechanism now activated in Unit 1, and with Unit 2 suffering widespread damage from the previous runs, the test was concluded to prevent the specimen from collapsing on the shake table.

5.2 Interface behaviour

The behaviour of the interface between the units of the aggregate was captured using the Optotrak optical device and LED markers, as described in Sect. 4. The precision of the

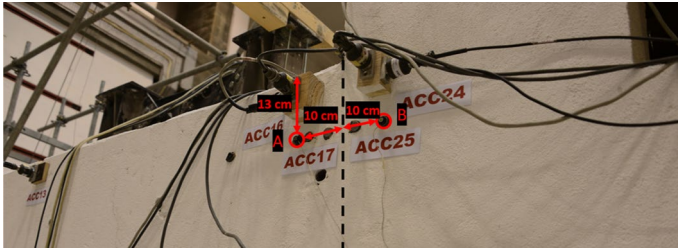


Fig. 21 Position of Optotrak markers on facade 3 used to calculate relative displacements at the interface between the units

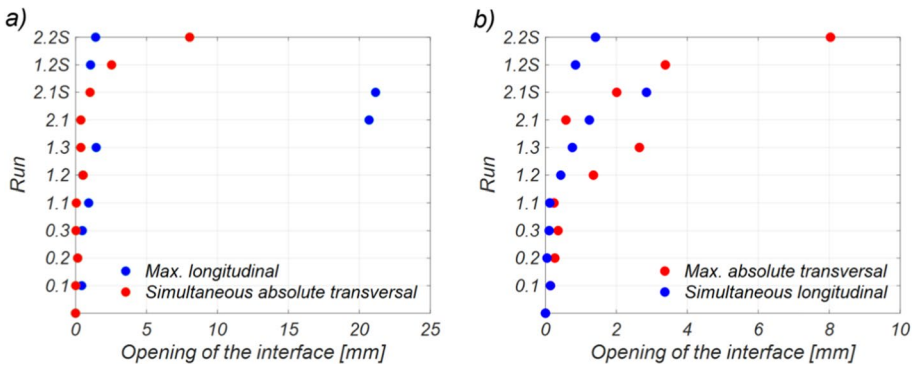


Fig. 22 Openings of the interface joint: **a** Peak values in longitudinal (blue) with simultaneous absolute values in transverse (red) directions; **b** Peak absolute values in transverse (red) with simultaneous values in longitudinal (blue) directions

Optotrak device is under a millimetre, and the recording frequency was set to 200 Hz, which was considered sufficient to capture the effects of dynamic motion. Two markers were placed close to the top of the interface on facade 3, 10 cm away from the dry-joint on each side, as illustrated on Fig. 21.

The longitudinal (U_y) and transverse (U_x) openings of the interface joint between the units on facade 3 were calculated from the recordings of markers A and B, using Eqs. (1) and (2) in the global coordinate system, as defined in Fig. 2:

$$U_y = \Delta_y^B - \Delta_y^A, \tag{1}$$

$$U_x = \Delta_x^B - \Delta_x^A, \tag{2}$$

where Δ_y^i and Δ_x^i stand for the i -th marker displacement in the global y - or x -direction, respectively. Consequently, a positive sign of the transverse opening implies that the marker on Unit 2 moves more in the global positive x -direction than the one on Unit 1. A positive value of the longitudinal opening implies separation, and a negative value implies pounding between the units.

Figure 22 shows the peak values of interface joint opening in the longitudinal and transverse directions as well as the simultaneous opening of the interface in the other direction. For each maximum absolute value of the transverse opening, the longitudinal opening

had always a positive value. This means the units were separated at that instant and there was no frictional force opposing the transverse relative displacement. Bidirectional loading (run 1.3) led to significantly larger maximum absolute transverse displacement than unidirectional loading in the transverse direction (run 1.2).

The maximum values of relative and residual displacements at the interface for each run are shown in Table 5. During the bidirectional run 1.3, the maximum longitudinal opening increased up to 1.45 mm, while the maximum positive and negative transverse opening reached 2.33 mm and 2.65 mm, respectively. This indicates the out-of-plane vibration of facades 2 and 3 of Unit 1, which was later confirmed by crack maps and illustrated in Fig. 20. During the same run, the negative longitudinal displacement of -0.58 mm at the interface showed that the units were already experiencing pounding.

The longitudinal opening of the interface joint became especially pronounced during run 2.1, when it reached 20.7 mm. During the same run, the largest negative displacement of -1.85 mm indicated significant pounding at the interface. The residual longitudinal displacement after run 2.1 was -0.46 mm, i.e., with the units in contact with each other. Run 2.1 with the strengthened specimen produced similar longitudinal displacement, with the maximum and minimum being 21.2 mm and -1.87 mm, respectively. The residual longitudinal displacement reached 0.31 mm, with the units now separated.

The largest transverse displacement at the interface was observed during run 2.2S with the maximum absolute value of 8.04 mm. After the same run, the residual transverse displacement was -0.94 mm, which was the largest residual value observed on the interface in either direction.

5.3 In-plane response of facades

The three-dimensional optical LED acquisition systems enabled monitoring of the in-plane response of the longitudinal facades. As previously described, a clear flexural-rocking mechanism developed in Unit 2 with extensive cracking of the spandrels and piers. The in-plane horizontal elongation of the facades was calculated as a difference in displacements of the Optotrak markers at two corners of facade 3 for Unit 2. For Unit 1, the elongations were calculated as a difference in displacements of the Optotrak and Hamamatsu markers

Table 5 Maximum, minimum, and residual relative displacements at the interface of the two units

	Run ID	Longitudinal			Transversal		
		Max [mm]	Min [mm]	Residual [mm]	Max [mm]	Min [mm]	Residual [mm]
Unstrengthened	0.1	0.43	-0.09	0.02	0.12	-0.14	0.04
	0.2	0.15	-0.05	0.02	0.26	-0.26	-0.01
	0.3	0.47	-0.09	0.03	0.36	-0.22	0.02
	1.1	0.92	-0.20	0.1	0.14	-0.24	-0.03
	1.2	0.51	-0.06	0.16	0.87	-1.35	-0.08
	1.3	1.45	-0.58	0.21	2.33	-2.65	-0.13
	2.1	20.69	-1.85	-0.46	0.56	-0.58	-0.07
Strengthened	2.1S	21.15	-1.87	0.31	2.01	-0.41	0.39
	1.2S	1.05	-0.02	0.13	3.28	-3.38	0.14
	2.2S	1.41	-0.02	0.22	5.40	-8.04	-0.94

Fig. 23 Markers used to calculate the in-plane facade elongations

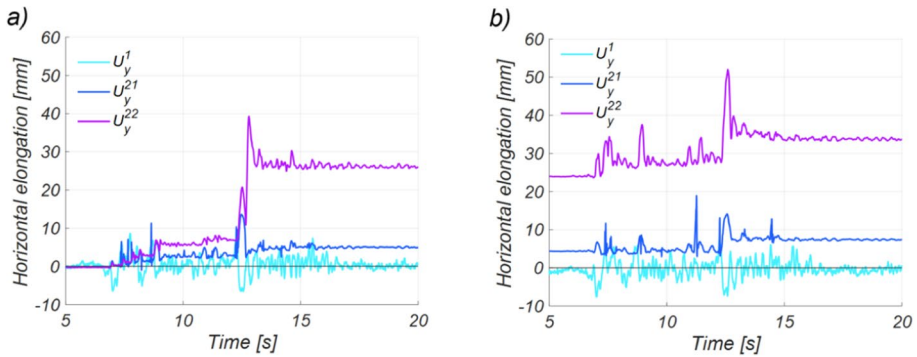
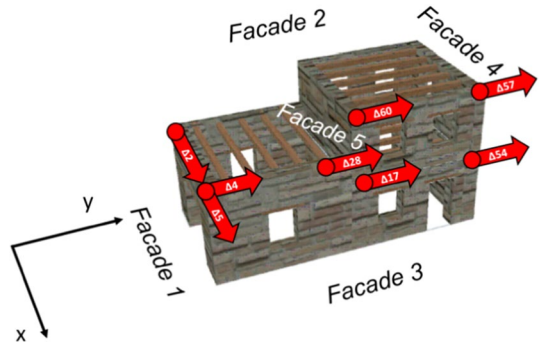


Fig. 24 Time history of the longitudinal elongation of facade 3 for Units 1 and 2: **a** Run 2.1; **b** Run 2.1S

at the two corners of facades 1 and 2. Figure 23 shows the displacements used to calculate the facade elongations according to Eqs. (3) through (6):

$$U_y^1 = \Delta_y^{28} - \Delta_y^4, \tag{3}$$

$$U_x^1 = \Delta_x^5 - \Delta_x^2, \tag{4}$$

$$U_y^{21} = \Delta_y^{54} - \Delta_y^{17}, \tag{5}$$

$$U_y^{22} = \Delta_y^{57} - \Delta_y^{60}, \tag{6}$$

where U_y^1 is the longitudinal façade elongation of Unit 1; U_y^{21} and U_y^{22} the longitudinal facade elongations of Unit 2 at the 1st and 2nd floor, respectively; and U_x^1 the transverse facade elongation of Unit 1. Δ_y^i and Δ_x^i are the i -th marker displacement in the global y - or x -direction, respectively.

Figure 24a presents the recorded time histories of longitudinal elongations for both units in run 2.1, with a PGA of 0.593 g. There were no residual elongations prior to this run in both units. In Unit 2 the elongation was greater at the 2nd storey, compatibly with the out-of-plane tendency of facade 4, that involved the end piers of the longitudinal facade as webs. This

resulted in a residual elongation of approximately 26.0 mm. Residual elongations of the 1st storey of Unit 1 and Unit 2 were approximately 0.3 mm and 5.0 mm, respectively.

Figure 24b presents the recorded time histories of the longitudinal elongations for both units from run 2.1S, with a PGA of 0.615 g. The floor-to-wall connections of Unit 2 were retro-fitted prior to this run, thus limiting the cumulation of residual deformations. Like the previous run, the elongation was greater at the 2nd storey of Unit 2, but the residual value increased by only 7.4 mm to a total of approximately 33.4 mm. Residual elongations of the 1st storey of Unit 1 and Unit 2 were approximately -0.74 mm and 7.4 mm, respectively, with increments of -1.04 mm and 2.4 mm.

For the last two transverse runs (run 1.2S and run 2.2S), the time-histories of the elongation of facade 1 are shown in Fig. 25. Residual values were approximately 1.4 mm and 4.7 mm for run 1.2S and run 2.2S, respectively. This confirms the observed behaviour of Unit 1, with the formation of the first cracks and the development of the transverse flexural-rocking mechanism during run 2.2S.

The LVDT data at the beam supports indicated progressive slippage, caused by the cumulative elongation of the longitudinal facades first, followed by that of the transverse ones.

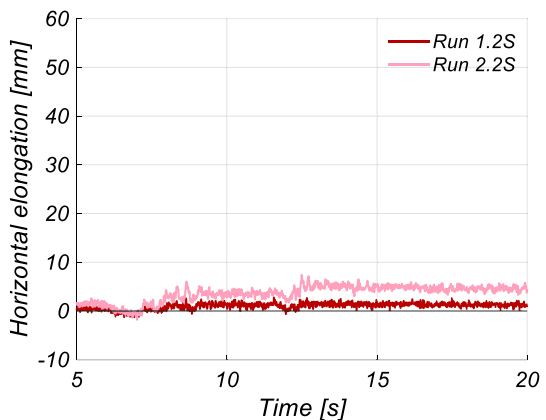
5.4 Force–displacement hysteretic response

Hysteretic curves were plotted for the entire structure in terms of base-shear coefficient (BSC) versus global drift ratio. Base-shear values were calculated by assigning tributary masses to each accelerometer in both directions. Tributary masses were multiplied by the recorded and filtered accelerations. The base shear (V_B) and the BSC were defined considering the full mass of the specimen; the mass of the lower half of the 1st storey walls was assumed to move rigidly with the table, and was multiplied with the shake table accelerations. Accordingly, V_B and BSC are given by Eq. 7:

$$BSC = \frac{V_B}{g \cdot m_{TOT}} = \frac{\sum_{i=1}^n (a_i \cdot m_i) + a_{st} \cdot m_{st}}{g \cdot (\sum_{i=1}^n m_i + m_{st})}, \tag{7}$$

where a_i is the acceleration recorded by the i th accelerometer and m_i is the tributary mass assigned to it; a_{st} is the shake table acceleration and m_{st} is the mass of the lower half of the 1st storey walls.

Fig. 25 Time history of the transverse elongation of facade 1 of Unit 1



The global drift ratio ($\tilde{\theta}_{j,AVG}$) represents the average displacement at the top of a unit divided by the total height of a unit, as given by Eq. 8:

$$\tilde{\theta}_{j,AVG} = \frac{\sum_{i=1}^n \Delta_i}{n \cdot h_j}, \tag{8}$$

where j identifies the structural unit (either 1 or 2), h_j is the total height of the unit (3.15 m for Unit 2 or 2.20 m for Unit 1), Δ_i is the displacement of the i -th marker or potentiometer at the top of a unit, and n is the total number of markers at the unit's top. Figure 26 shows the markers that were used to calculate the global drift ratios for the two structural units.

The hysteretic response for run 1.3, the strongest bidirectional run, is shown in Fig. 27. The hysteretic response of both units in both directions shows energy dissipation. At the same time, the only damage detected at the units after this run was cracking and separation at the interface.

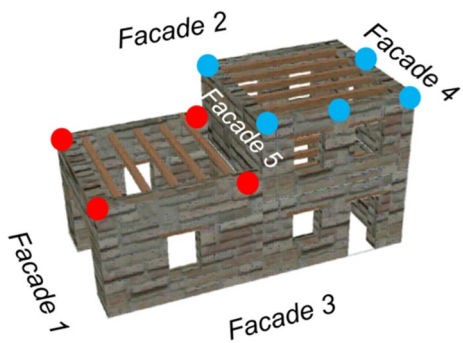
Figure 28 shows the hysteretic response for run 2.1 in the longitudinal y -direction. The formation of a soft-storey mechanism in the upper storey of Unit 2 resulted in anelastic hysteretic response, reaching global drift-ratio values greater than 1.5%. Figure 29 illustrates the behaviour for run 2.1S, where accumulated damage increased the global drift ratio of Unit 2 to values above 3%, even if retrofitted.

For the higher seismic intensity (run 2.1 and run 2.1S), the 1st storey drift ratio in the y -direction was significantly lower than the global drift ratio due to the soft-storey flexural mechanism forming in the 2nd storey of Unit 2. This behaviour was possibly emphasized by the interaction with a lower, stiffer and stronger structural unit, that did not show large drift values either. The effects of pounding between the two units are visible as sudden spikes in the hysteretic loops.

Finally, the hysteretic response during the strongest transverse x -direction run is shown in Fig. 30. It confirms the onset of a rocking mechanism in Unit 1, with slight loss of strength in large-amplitude cycles of increasing displacement demand.

Table 6 summarizes the maximum global drift-ratio values per run for both units in both directions.

Fig. 26 Markers used to calculate global drift ratios: red for Unit 1, blue for Unit 2



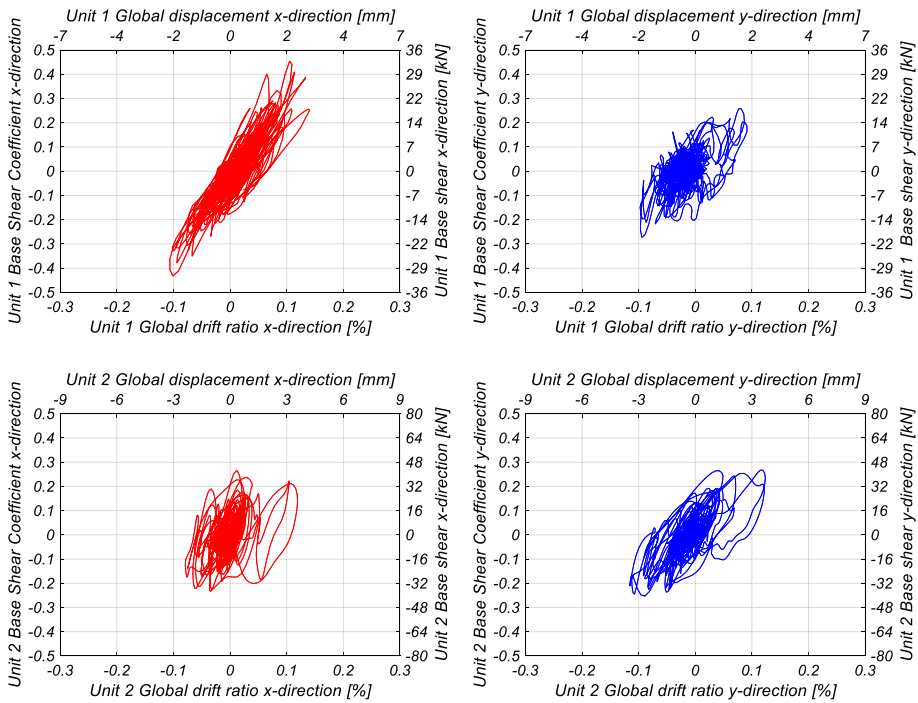


Fig. 27 Hysteretic responses in both directions for run 1.3

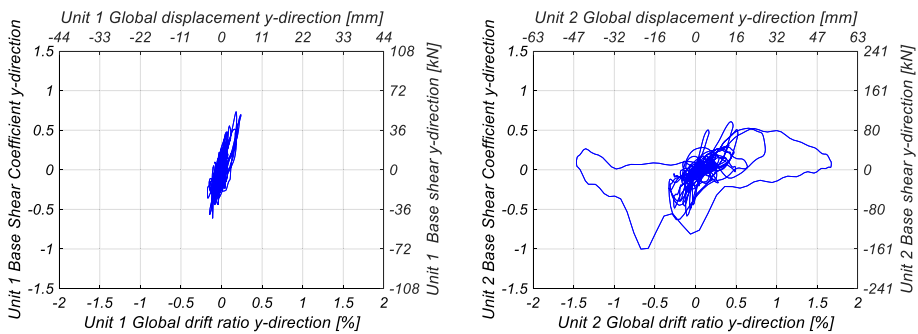


Fig. 28 Hysteretic responses in the y-direction for run 2.1

6 Conclusions

This paper presented the half-scale bidirectional shake table test of a two-units stone masonry building aggregate. The specimen was built of undressed double-leaf stone masonry with poor interlocking to replicate a typical historical construction. A two-storey unit was constructed first, and mortar was applied at the interface with the adjacent unit to prevent any interlock between stones. Finally, the adjacent one-storey unit was completed. Timber beams and a layer of planks formed the floors, resulting in flexible diaphragms.

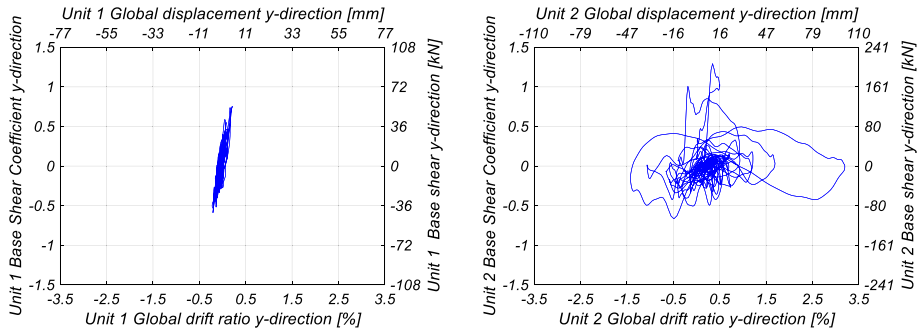


Fig. 29 Hysteretic responses in the y-direction for run 2.1S

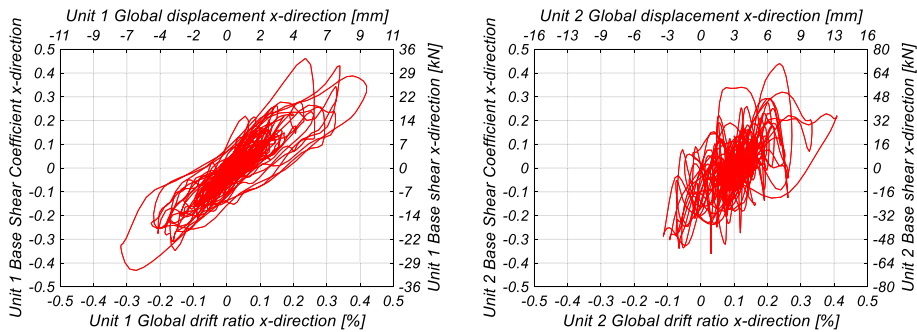


Fig. 30 Hysteretic responses in the x-direction for run 2.2S

Table 6 Maximum global drift-ratio values for both units in both directions

Run ID	Unit 1		Unit 2	
	Transverse drift-ratio [%]	Longitudinal drift-ratio [%]	Transverse drift-ratio [%]	Longitudinal drift-ratio [%]
0.1	0.04	0.06	0.03	0.07
0.2	0.05	0.03	0.04	0.02
0.3	0.05	0.06	0.06	0.07
1.1	0.04	0.08	0.05	0.12
1.2	0.07	0.05	0.07	0.03
1.3	0.14	0.10	0.12	0.12
2.1	0.09	0.24	0.16	1.67
2.1S	0.10	0.22	0.29	3.20
1.2S	0.16	0.06	0.21	0.27
2.2S	0.42	0.06	0.41	0.32

The project had two main goals: (i) investigating experimentally the role of the interface on the aggregate behaviour, (ii) producing high-quality data for the validation of numerical models. The loading sequence consisted of orthogonal unidirectional and simultaneous

bidirectional shake table runs of increasing intensity. The building prototype experienced its first visible damage in the form of a vertical crack at the interface between the units for a PGA of 0.170 g in the longitudinal direction.

Extensive damage on the two-storey unit was reached during the unidirectional longitudinal run with PGA of 0.593 g. Interaction with the adjacent shortest unit forced the development of a soft-storey mechanism at the 2nd storey of the tallest unit, while the 1st storey and the shortest unit did not undergo large drift ratios. Both piers and spandrels suffered extensive flexural cracking in the longitudinal facades at the 2nd story, with permanent horizontal elongations of the spandrels. The mechanism included significant out-of-plane displacements and cracking on the transverse facades. Cracks were continuous and connected across orthogonal walls because, due to interlocking between orthogonal walls, the end piers of the longitudinal facades acted as webs in the out-of-plane overturning mechanism of the transverse walls.

To protect against out-of-plane collapse after the full activation of the 2nd storey mechanism, the tallest unit was strengthened by improving beam-to-wall connections, and testing was resumed by repeating the longitudinal run at the same intensity. Existing damage mechanisms progressed, but out-of-plane collapse was effectively prevented. When applying the input motion in the transverse direction, the shortest unit exhibited out-of-plane vibrations of the longitudinal walls, especially close to the edges not connected to the transverse wall. This mechanism might become particularly relevant in the absence of interlock between the structural units.

The interface behaviour was one of the main focuses of this test campaign. Optical markers, installed adjacent to the interface, recorded relative displacements of the joint in both longitudinal and transverse directions. In the longitudinal direction, the specimen exhibited both pounding and separation. In the transverse direction, the largest absolute relative displacements always occurred at instants when the units were longitudinally separated. This suggests that friction forces across the interface were sufficiently large to reduce the magnitude of the relative transverse displacement when the joint was closed. This behaviour could be observed thanks to bidirectional loading.

The outcomes of the shake-table test show that the observed experimental behaviour can be replicated only by explicitly modelling the connection between the units, including both normal and frictional characteristic of the contact interface. Moreover, the complexities emerged in the dynamic responses of each structural unit and of the contact interface make further three-dimensional shake table tests necessary to better understand the seismic behaviour of aggregates, to calibrate numerical models, and to define practical strategies to account for the interaction.

Acknowledgements The authors would like to thank the technicians of the LNEC laboratory in Lisbon whose dedicated work allowed the project run smoothly and across all the obstacles: Artur Santos, Susana Almeida, Aurélio Bernardo, and Anabela Martins. We owe our thanks to master students whose efforts helped the project: Cecilia Noto and Samuel Cosme. Finally, want to stress the contribution of post-doctoral researcher Filipe Luis Ribeiro to the successful outcome of the project.

Funding Open access funding provided by EPFL Lausanne. Open access funding provided by EPFL Lausanne. The project leading to this paper has received funding from the European Union's Horizon 2020 research and innovation programme under Grant Agreement No 730900 of The Seismology and Earthquake Engineering Research Infrastructure Alliance for Europe (SERA), under the name SERA - Adjacent Interacting Masonry Structures (AIMS). The first author of this project was partially funded through the project grant 200021_175903/1 "Equivalent frame models for the in-plane and out-of-plane response of unreinforced masonry buildings" supported by the Swiss National Science Foundation.

Data availability Raw experimental data, files used to process raw data, processed data, and files used to produce the figures presented in this paper can be accessed through the repository <https://doi.org/10.5281/zenodo.6546434>.

Competing Interests The authors have not disclosed any competing interests.


Open Access This article is licensed under a Creative Commons Attribution 4.0 International License, which permits use, sharing, adaptation, distribution and reproduction in any medium or format, as long as you give appropriate credit to the original author(s) and the source, provide a link to the Creative Commons licence, and indicate if changes were made. The images or other third party material in this article are included in the article's Creative Commons licence, unless indicated otherwise in a credit line to the material. If material is not included in the article's Creative Commons licence and your intended use is not permitted by statutory regulation or exceeds the permitted use, you will need to obtain permission directly from the copyright holder. To view a copy of this licence, visit <http://creativecommons.org/licenses/by/4.0/>.

References

- Benedetti D, Petrini V (1984) On the seismic vulnerability of masonry buildings: an evaluation method (in Italian). *L'industria Delle Costr* 149:66–74
- Benedetti D, Carydis P, Pezzoli P (1998) Shaking table tests on 24 simple masonry buildings. *Earthq Eng Struct Dyn* 27:67–90
- Buckingham E (1914) On physically similar systems; illustrations of the use of dimensional equations. *Phys Rev* 4:345
- Carocci CF (2012) Small centres damaged by 2009 L'Aquila earthquake: on site analyses of historical masonry aggregates. *Bull Earthq Eng* 10:45–71. <https://doi.org/10.1007/s10518-011-9284-0>
- Coutinho CP, Baptista AJ, Rodrigues JD (2016) Reduced scale models based on similitude theory: a review up to 2015. *Eng Struct* 119:81–94
- Croci G, Viskovic A, Herzalla A et al (2010) Seismic assessment by numerical analyses and shaking table tests for complex masonry structures: the Hagia Irene case study. *Advanced materials research. Trans Tech Publ, Stafa-Zurich*, pp 777–782
- da Porto F, Munari M, Prota A, Modena C (2013) Analysis and repair of clustered buildings: case study of a block in the historic city centre of L'Aquila (Central Italy). *Constr Build Mater* 38:1221–1237. <https://doi.org/10.1016/j.conbuildmat.2012.09.108>
- Formisano A (2017) Theoretical and numerical seismic analysis of masonry building aggregates: case studies in San Pio Delle Camere (L'Aquila, Italy). *J Earthq Eng* 21:227–245. <https://doi.org/10.1080/13632469.2016.1172376>
- Formisano A, Massimilla A (2018) A novel procedure for simplified nonlinear numerical modeling of structural units in masonry aggregates. *Int J Archit Herit* 12:1162–1170. <https://doi.org/10.1080/15583058.2018.1503365>
- Formisano A, Florio G, Landolfo R, Mazzolani FM (2015) Numerical calibration of an easy method for seismic behaviour assessment on large scale of masonry building aggregates. *Adv Eng Softw* 80:116–138. <https://doi.org/10.1016/j.advengsoft.2014.09.013>
- Guerrini G, Senaldi I, Graziotti F et al (2019) Shake-table test of a strengthened stone masonry building aggregate with flexible diaphragms. *Int J Archit Herit* 13:1–20. <https://doi.org/10.1080/15583058.2019.1635661>
- Guerrini G, Senaldi I, Scherini S et al (2017) Material characterization for the shaking-table test of the scaled prototype of a stone masonry building aggregate. In: XVII convegno ANIDIS, Pistoia, Italy
- Krawinkler H, Moncarz P (1981) Theory and application of experimental model analysis in earthquake engineering. NASA STI/Recon Tech Rep N 82:18430
- Lagomarsino S, Penna A, Galasco A, Cattari S (2013) TREMURI program: an equivalent frame model for the nonlinear seismic analysis of masonry buildings. *Eng Struct* 56:1787–1799. <https://doi.org/10.1016/j.engstruct.2013.08.002>
- Luzi L, Puglia R, Russo E (2016) Engineering strong motion database, version 1.0 istituto nazionale di geofisica e vulcanologia. Observatories & Research Facilities for European Seismology, Rome
- Magenes G, Kingsley GR, Calvi GM (1995) Seismic testing of a full-scale, two-story masonry building: test procedure and measured experimental response. Department of structural mechanics. University of Pavia, Pavia

- Magenes G, Penna A, Senaldi IE, Rota M, Galasco A (2014) Shaking table test of a strengthened full-scale stone masonry building with flexible diaphragms. *Int J Archit Herit* 8:349–375. <https://doi.org/10.1080/15583058.2013.826299>
- Maio R, Vicente R, Formisano A, Varum H (2015) Seismic vulnerability of building aggregates through hybrid and indirect assessment techniques. *Bull Earthq Eng* 13:2995–3014. <https://doi.org/10.1007/s10518-015-9747-9>
- Malcata M, Ponte M, Tiberti S, Bento R, Milani G (2020) Failure analysis of a portuguese cultural heritage masterpiece: bonet building in sintra. *Eng Fail Anal* 115:104636
- Mazzon N, Chavez CM, Valluzzi MR, Casarin F, Modena C (2010) Shaking table tests on multi-leaf stone masonry structures: analysis of stiffness decay. *Advanced materials research*. Trans Tech Publ, Stafa-Zurich, pp 647–652
- McKenna F, Fenves GL, Scott MH, Jeremic B (2000) Open system for earthquake engineering simulation (OpenSees). University of California, Berkeley, CA
- Moss RES, Crosariol VA (2013) Scale model shake table testing of an underground tunnel cross section in soft clay. *Earthq Spectra* 29:1413–1440
- Mouzakis C, Adami C-E, Karapitta L, Vintzileou E (2018) Seismic behaviour of timber-laced stone masonry buildings before and after interventions: shaking table tests on a two-storey masonry model. *Bull Earthq Eng* 16:803–829
- Penna A, Lagomarsino S, Galasco A (2014) A nonlinear macroelement model for the seismic analysis of masonry buildings. *Earthq Eng Struct Dynam* 43:159–179. <https://doi.org/10.1002/eqe.2335>
- Senaldi I, Magenes G, Penna A (2010) Numerical investigations on the seismic response of masonry building aggregates. *Advanced materials research*, vol 133. Trans Tech Publications Ltd, Stafa-Zurich, pp 715–720
- Senaldi I, Magenes G, Penna A et al (2014) The effect of stiffened floor and roof diaphragms on the experimental seismic response of a full-scale unreinforced stone masonry building. *J Earthq Eng* 18:407–443. <https://doi.org/10.1080/13632469.2013.876946>
- Senaldi I, Guerrini G, Comini P, Graziotti F, Penna A, Beyer K, Magenes G (2019a) Experimental seismic performance of a half-scale stone masonry building aggregate. *Bull Earthq Eng*. <https://doi.org/10.1007/s10518-019-00631-2>
- Senaldi I, Guerrini G, Scherini S, Morganti S, Magenes G, Beyer K, Penna A (2018) Natural stone masonry characterization for the shaking-table test of a scaled building specimen. In: *Proceedings of the 10th international masonry conference*, Milan, Italy, pp 9–11
- Senaldi I, Guerrini G, Solenghi M, Graziotti F, Penna A (2019b) Numerical modelling of the seismic response of a half-scale stone masonry aggregate prototype. In: *XVIII convegno ANIDIS*, Ascoli Piceno, Italy
- Stavroulaki ME (2019) Dynamic behavior of aggregated buildings with different floor systems and their finite element modeling. *Front Built Environ* 5:138. <https://doi.org/10.3389/fbuil.2019.00138>
- S.T.A. Data (2008) 3muri. Seismic calculation of masonry structures according to the Italian ministerial decree 14
- Sullivan TJ, Pinho R, Pavese A (2004) An introduction to structural testing techniques. *Earthq Eng Res Rep Rose Sch* 1:1–200
- Tomažević M, Weiss P, Velechovsky T (1991) The influence of rigidity of floors on the seismic behaviour of old stone-masonry buildings
- Vanin F, Penna A (2020) Beyer K 1 a three-dimensional macroelement for the modelling of in-plane and out-of-plane 2 response of masonry walls. *Earthq Eng Struct Dyn* 49(14):1365–1387
- Vanin F, Penna A, Beyer K (2020) Equivalent-frame modeling of two shaking table tests of masonry buildings accounting for their out-of-plane response. *Front Built Environ* 6:42. <https://doi.org/10.3389/fbuil.2020.00042>
- Vintzileou E, Mouzakis C, Adami C-E, Karapitta L (2015) Seismic behavior of three-leaf stone masonry buildings before and after interventions: shaking table tests on a two-storey masonry model. *Bull Earthq Eng* 13:3107–3133. <https://doi.org/10.1007/s10518-015-9746-x>
- Zheng D, Liu F, Ju N et al (2016) Cyclic load testing of pre-stressed rock anchors for slope stabilization. *J Mt Sci* 13:126–136

Authors and Affiliations

I. Tomić¹ · A. Penna² · M. DeJong³ · C. Butenweg⁴ · A. A. Correia⁵ · P. X. Candeias⁵ ·
I. Senaldi⁶ · G. Guerrini² · D. Malomo⁷ · K. Beyer¹ 

✉ K. Beyer
katrin.beyer@epfl.ch

¹ Earthquake Engineering and Structural Dynamics Laboratory (EESD), École Polytechnique Fédérale de Lausanne (EPFL), School of Architecture, Civil and Environmental Engineering (ENAC), Lausanne, Switzerland

² Department of Civil Engineering and Architecture (DICAr), University of Pavia, Pavia, Italy

³ Department of Civil and Environmental Engineering, University of California Berkeley, Berkeley, USA

⁴ Center for Wind and Earthquake Engineering, RWTH Aachen University, Aachen, Germany

⁵ National Laboratory for Civil Engineering (LNEC), Lisbon, Portugal

⁶ European Centre for Training and Research in Earthquake Engineering (EUCENTRE), Pavia, Italy

⁷ Department of Civil Engineering, McGill University, Montreal, Quebec, Canada